Khelef *et al.*
Journal of Engineering and Applied Science (2022) 69:73
https://doi.org/10.1186/s44147-022-00121-4

Journal of Engineering and Applied Science

RESEARCH Open Access

Numerical calculation of temperature, velocity, and species concentration distributions in a hot filament chemical vapor deposition in a reactor using a CH_4/H_2 mixture

Nour Khelef, Fethi Khelfaoui* and Oumelkheir Babahani

*Correspondence:
fethi.khelfaoui@gmail.com;
khelfaoui.fethi@univ-ouargla.dz

Faculté des Mathématiques et Sciences de la Matière, Laboratoire Rayonnement et Plasmas et Physique des Surfaces (LRPPS), Université Kasdi Merbah Ouargla, 30000 Ouargla, Algeria

Abstract

This study is a numerical modeling of transport phenomena occurring in the reaction chamber during diamond or amorphous hydrogenated carbon films growth by a hot filament chemical vapor deposition (HFCVD) technique. A two-dimensional model was adopted to study the HFCVD reactor. The equations of heat, momentum, and mass transfer were solved numerically; the simulation was performed using a program in FORTRAN language. All temperature, velocity, and species concentration distributions were similar at the filaments and they were also similar between the filaments. The results show that the gas temperature increases when the number of filaments increases from three to four filaments. We also noted an increase in the production of CH_3 and C_2H_5 radicals near the surface; there was also an increase in the growth rate of the thin film. The concentrations of C_2H_6, C_2H_4, and C_2H_5 were very high. Temperature and concentrations were affected by the distance between filaments and the distance filaments-substrates.

Keywords: Chemical vapor deposition, Fluid model, Finite volume method, Gauss-Seidel method, CH_4/H_2 gas mixture, Chemical reaction, Diffusion, Concentration, Thin film deposition

Introduction

Thin films based on diamond or on hydrogenated amorphous carbon (a-C:H) present many technological interests: a-C:H films are commonly used, for example, in organic printable electronic devices [1]. They can be used as protective and antireflection films on optical instruments and on solar cells [2, 3]. They can also be used in optoelectronic device [4] to develop sensors (LED: Light-Emitting Diode), electrochemical detectors, bioelectronic and bioelectrochemical applications [5–8].

These thin films can be produced by chemical vapor deposition (CVD) using a CH_4/H_2 gas mixture, in which H_2 is dissociated into atomic H and CH_4 undergoes pyrolysis reactions leading to the formation of radicals such as CH_3 and CH_2 and stable species such as C_2H_2, C_2H_4, and C_2H_6 [9]. Activation of chemical reactions can occur at elevated

temperatures, up to 3000 K in plasmachemical processes [10]. The radicals H and CH_3 are very important for the mechanisms of deposition [11].

The hot filament chemical vapor deposition (HFCVD) technique is very suitable because it is economic and scalable to large areas [12]. The HFCVD technique is very popular as it allows coating of complex shapes and internal surfaces, with a low operating cost [13]. An advantage of hot filament CVD reactors over the other reactors is the simplicity of the system and the uniform diamond deposition over a large area. HFCVD is a simple and a reproducible way to grow diamond at low pressures. It is also the first method to achieve nucleation and continuous growth of diamond on various substrates [9].

Diamond carbon can be deposited on a substrate made of Si, Mo, or silica, etc., which is mounted at a distance of 0.5 to 2 cm from the glowing filament and kept at 700 to 1000 °C either by the radiation from the filament or by a separate substrate heater [9]. A group of parallel filaments can be arranged in single or multiple parallel planes and in horizontal or vertical orientation [14].

In the HFCVD process, the production of thin films depends on substrate and gas temperatures and the velocity and volume density of gas as well as on complex chemical reactions of the gas phase [15]. Goodwin and Gavillet [16] developed the first one-dimensional numerical model for the diamond growth. They calculated temperature, velocity, and species concentration profiles. Debroy et al. [17] developed the first two-dimensional model of the HFCVD process. The authors showed that diffusion mechanisms are mostly responsible for both heat and mass transfer inside the reaction chamber. Some studies have focused on the concentrations of different species and radicals, in particular CH_3, and the growth rate of thin layers of diamonds [18–20]. One-dimensional models [21, 22] were developed to understand the deposition processes and the gas-phase behavior. Other numerical studies about two- and three-dimensional models [17, 19, 23–27] were interested in studying the effect of the parameters such as reactor geometry, the diameter, the number of the filaments, and the separation between hot filaments in the growth process of diamond films. These numerical models allow the creation of simplified models to reduce experiences that are often expensive [10].

Many other works [28–33] were focused on several aspects related to HFCVD processes (physical parameters of gas, gas-phase diffusion, chemical reaction rates, equilibrium constants, concentrations of species, filament temperature, filament geometry, filament arrangement, deposition parameters…); these factors can affect the growth of thin films.

In experimental and calculation work, Kondoh et al. [18] studied the effect of some HFCVD parameters on diamond growth in CH_4/H_2 gas mixture. Spatial distributions of the gas temperature, fluid velocity, and chemical species concentrations have been calculated in a two-dimensional HFCVD system for CH_4/H_2 gas mixture [18]. The partial differential equations used were those of conservation of mass, momentum, energy, and chemical species. May et al. [20] studied mechanism of growth in diamond films using $A_r/CH_4/H_2$ gas mixtures in the HFCVD reactor. They used a two-dimensional computer model to calculate the gas-phase composition within the reactor. Using experimental and calculated data, they showed the competition between H atoms, CH_3 radicals, and other species film morphology. Eckert et al. [34] were interested in the calculation of the sticking coefficients of species CH_x (x: 0–4), C_2H_x (x: 0–6), C_3H_x (x: 0–2), C_4H_x (x: 0–2),

H, and H_2 on clean and hydrogenated diamond. They used the molecular dynamic simulation method.

In recent work, Tao Zhang et al. [35] presented a three-dimensional model for depositing the diamond films by a hot filament CVD. Their simulation model coupled heat transfer mechanisms by radiation, by conduction, and by convection. The authors showed that the thermal conductivity influences the temperature. Rebrov et al. [36] and Gorbachev et al. [37] studied the impact of gas-phase reactions on characteristics of the flow in a heated cylindrical channel of a gas mixture CH_4/H_2 reactor with using the direct simulation Monte Carlo method which is a method based on solving the Navier-Stokes equations. The study shows the complexity of the influence of the various physical and geometric parameters on the concentrations and on the deposition.

In this work, we present a two-dimensional model for HFCVD, for a gas mixture CH_4/H_2. This model studies distributions of temperature, velocity, and species concentration and the effect of the number of filaments and their distance from substrate. The proposed geometry of the reactor is different from several shapes cited in the literature. Numerical simulation can give extensive information about effect of several factors on gas mixture of HFCVD process.

The proposed reactor has two substrates of horizontal form. Long, equidistant and coplanar hot filaments are parallel to the substrates. The gas mixture enters the reactor with a constant flow. The fluid is considered Newtonian and the flow is laminar. We use the fluid model in the two-dimensional stationary regime to calculate spatial distributions of gas velocity and gas temperature and species concentrations.

In the second section, we present the principal equations of the mathematical model and the proposed calculation method. We use the nonlinear stationary differential equations: Navier-Stokes equations and continuity equation for velocity, heat equation for temperature, and equation of diffusion for concentrations. In the third section, we present the numerical model based on the finite volume method (FVM) with an adequate choice of boundary conditions. The results of this work are presented in the fourth section. Spatial distributions of velocities, temperature, and species concentrations are calculated for a gas mixture CH_4/H_2 with discussion and comments. First, we present distributions of velocity and temperature for three and four filaments. In the next step, we present species concentrations in volume, effects of number of filaments, and effects of distance filaments-substrates. In this fourth section, we also present concentrations of CH_3, C_2H_5, and H near the substrates. As an application, an estimation of the growth rate of deposited thin film is made. The last section includes the conclusion of this work and the future prospects.

Methods and mathematical model

The principal aim is calculation of distributions of temperature, velocity, and species concentration in an HFCVD process. The considered HFCVD reactor has two openings for the inlet and outlet gas. The substrates are horizontal plates; they have a constant temperature T_{sub}. Let L be the length of the reactor in the x direction and let Z_{max} be the distance between substrates. Long, equidistant and coplanar hot filaments are parallel to the substrates. In the HFCVD reactor, there are "n" filaments which are heated to a same temperature T_{fil}. The distance between two filaments is D_{ff}. A gas mixture CH_4/H_2 enters the reactor

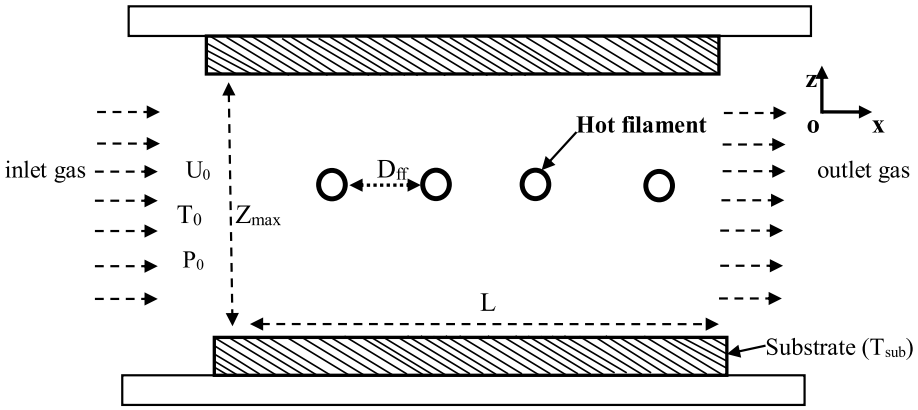

Fig. 1 Simplified scheme of the HFCVD reactor

Table 1 Values of parameters used for the reactor

Parameter	Typical values
Filament temperature (K)	2100
Substrate temperature (K)	1173
Initial temperature of gas (K)	300
Pressure (Pa)	1000
Inlet velocity (mm s^{-1})	10
Length of the reactor in the *x* direction (mm)	240
Distance between substrates (mm)	20
Distance between three filaments (mm)	50
Distance between four filaments (mm)	33.3
Inlet gas composition CH_4/H_2	05–95%

with a constant flow in the x direction. The initial composition of the mixture gas is 5% of methane CH_4 and 95% of hydrogen H_2. The given initial temperature, velocity, and pressure are respectively T_0, U_0, and P_0. The v*olumetric* mass *density* ρ_0 is given according to ideal gas state equation as $\rho_0 = P_0/RT_0$, where R is the gas constant. A simplified scheme of the HFCVD reactor used in the model is shown in Fig. 1. Table 1 presents values of parameters used for the reactor. A numerical study of the phenomena is required.

For the mathematical model, we consider a gas mixture in two-dimensional coordinates in stationary regime (independent of time). We assume that the substrates are wide enough (direction y) so that this space dimension does not affect the results. We use the fluid model: the fluid is considered Newtonian and the flow is laminar; the effect of radiation has not been taken into account. The flow gas in the reactor obeys the conservation laws of mass (continuity equation) Eq. (1), momentum (Navier-Stokes equations) (Eq. (2) and Eq. (3)), and energy diffusion equation Eq. (4). To calculate gas velocity and gas temperature, we use the following nonlinear differential equations:

$$\operatorname{div}\left(\rho \vec{V}\right) = 0 \tag{1}$$

$$\rho U\frac{\partial U}{\partial x}+\rho W\frac{\partial U}{\partial z}=-\frac{\partial p}{\partial x}+\mu\left(\frac{\partial^2 U}{\partial x^2}+\frac{\partial^2 U}{\partial z^2}\right)+\rho g_x \tag{2}$$

$$\rho U\frac{\partial W}{\partial x}+\rho W\frac{\partial W}{\partial z}=-\frac{\partial p}{\partial z}+\mu\left(\frac{\partial^2 W}{\partial x^2}+\frac{\partial^2 W}{\partial z^2}\right)+\rho g_z \tag{3}$$

$$\rho C_p\left(U\frac{\partial T}{\partial x}+W\frac{\partial T}{\partial z}\right)=\lambda\left(\frac{\partial^2 T}{\partial x^2}+\frac{\partial^2 T}{\partial z^2}\right) \tag{4}$$

where U and W are components of the velocity $\vec{V}$ on directions x and z respectively; T is the temperature of gas. The constants ρ, μ, λ, and C_p, are the volume density, the dynamic viscosity, the heat transfer efficiency, and the specific heat respectively. In this model, the various species considered in the calculations are nine species ($k_{\max}=9$): H_2, CH_4, H, CH_3, C_2H_2, C_2H_3, C_2H_4, C_2H_5, and C_2H_6. To resolve the concentration C_k of each radical or molecule ($k=1, 2, \ldots, k_{\max}$), we consider the equation of chemical species [38, 39]:

$$\vec{V}\,\overrightarrow{\mathbf{grad}}C_k=D_k\nabla^2 C_k+R_k \tag{5}$$

where D_k is the diffusivity of species k and R_k is its rate production (or consumption) in volume.

Table 2 presents the gas-phase reaction mechanism; these reactions were used in works of Olivas-Martinez et al. [15] and Mankelevich et al. [23]. The gas-phase reaction mechanism consists of 13 reactions. We calculate the variations of chemical rate constants K_r with the temperature T for interactions between molecules and radicals. The general form is $K_r=A_rT^{\beta}\exp(-E_a/RT)$, where A_r and β are constants, E_a is the reaction activation energy, and R is the gas constant. For the units, A_r is in mol cm^{-3} s^{-1}; E_a is in kJ mol^{-1}, T is in K, and R is in J mol^{-1} K^{-1}.

Table 2 Gas-phase reaction mechanism and corresponding rate constants

	Reaction	Rate constants $K_r=A_rT^{\beta}\exp(-E_a/RT)$ K_r (A_r, β, E_a)
R1	$C_2H_6 \rightarrow CH_3+CH_3$	$K_1(5.52\times10^{42}, -8.90, 452.09)$
R2	$CH_4 \rightarrow CH_3+H$	$K_2(1.34\times10^{33}, -6.18, 451.96)$
R3	$C_2H_5 \rightarrow C_2H_4+H$	$K_3(6.28\times10^{37}, -8.24, 186.89)$
R4	$C_2H_2+H \rightarrow C_2H_3$	$K_4(3.12\times10^{35}, -7.61, 31.73)$
R5	$CH_4+H \rightarrow CH_3+H_2$	$K_5(2.20\times10^{4}, 3.0, 36.63)$
R6	$CH_3+CH_3 \rightarrow C_2H_4+H_2$	$K_6(1.0\times10^{16}, 0, 133.10)$
R7	$CH_3+CH_4 \rightarrow C_2H_5+H_2$	$K_7(1.0\times10^{13}, 0, 96.29)$
R8	$C_2H_5+H \rightarrow CH_3+CH_3$	$K_8(1.0\times10^{14}, 0, 0)$
R9	$C_2H_3+H \rightarrow C_2H_2+H_2$	$K_9(4.0\times10^{13}, 0, 0)$
R10	$C_2H_4+H \rightarrow C_2H_3+H_2$	$K_{10}(1.1\times10^{14}, 0, 35.58)$
R11	$C_2H_6+H \rightarrow C_2H_5+H_2$	$K_{11}(5.4\times10^{2}, 3.5, 21.81)$
R12	$H+H+H_2 \rightarrow H_2+H_2$	$K_{12}(9.2\times10^{16}, -0.6, 0)$
R13	$CH_3+CH_3 \rightarrow C_2H_6$	$K_{13}(6.36\times10^{41}, -7.03, 11{,}56)$

The general chemical reaction is expressed as [40]:

$$a_1A_1 + b_1B_1 + .. \cdots \Rightarrow a_2A_2 + b_2B_2 + .. \ldots . \tag{6}$$

The general form of reaction rate is given by:

$$R_k = K_r(T)[A_i]^{a_i}[B_i]^{b_i} \ldots .$$

where $K_r(T)$ is the reaction rate constant, $[A_i]$, $[B_i]$ are the species concentrations, and a_i, b_i,..., are stoichiometric coefficients of chemical reactions. The diffusion coefficient D_k of a particle k in a gas can be calculated from the coefficient $D_{\mathrm{mm'}}$ of binary collisions between two species m and k using the formulas below [41–43]:

$$D_k = \frac{(C_{tot} - C_k)}{\left(\sum_{m=1, m\neq k}^{k_{\max}} \frac{C_m}{D_{km}} \right)} \tag{7}$$

where C_{tot} is the total concentration and D_{mk} is the diffusion coefficients of the neutral species k in each of the background gases m.

$$D_{mk} = \frac{3}{16} \frac{(4\pi K_b T/2M_{mk})^{1/2}}{C_{tot}\pi\sigma^2{}_{mk}\Omega_D(T^*)} \tag{8}$$

D_{mk} is in m^2/s, $C_{tot} = P/K_bT$ in m^{-3}, K_b is the Boltzmann constant (J K^{-1})

M_{mk} is the reduced mass $M_{mk} = \frac{M_m \times M_k}{M_m + M_k}$; σ_{mk} is the binary collision diameter $\sigma_{mk} = \frac{\sigma_m + \sigma_k}{2}$, and it is in Å.

$T^* = \frac{T}{\sigma_{mk}}$ with the binary collision diameter $\varepsilon_{mk} = (\varepsilon_m \times \varepsilon_k)^{1/2}$ in K. ε_m and ε_k are Lennard-Jones parameters.

$$\Omega_D(T^*) = \frac{A_D}{T^{*B_D}} + \frac{C_D}{e^{D_D T*}} + \frac{E_D}{e^{F_D T*}} + \frac{G_D}{e^{H_D T*}} \tag{9}$$

with $A_D = 1.06036$, $B_D = 0.15610$, $C_D = 0.19300$, $D_D = 0.47635$, $E_D = 1.03587$, $F_D = 1.52996$, $G_D = 1.76474$, $H_D = 3.89411$ [41, 42]:

The used values of Lennard-Jones parameters are cited in [44].

In the calculation, we take for the physical constants ρ, μ, λ, and C_p those of mixture gas where the composition is dominant; they are according to data used in [31]. The details of the method or the numerical modeling for the treatment of the problem are presented in the next section.

Numerical model and boundary conditions

The numerical model is based on the finite volume method (FVM) [45]. We discretize the spatial domain of the reactor at discrete nodes (points). Let be a constant step along x axis and let i be the index of the corresponding node; let be a constant step along z axis, and let j be the index of the corresponding node. As it is known in the FVM, we apply an integral around an elementary volume at the level of the node (i,j).

We apply FVM, to calculate the component U by resolving Navier-Stokes equation Eq. (2); the component W is deduced from continuity equation Eq. (1). We apply FVM, to calculate the temperature T by resolving heat equation Eq. (4). We apply FVM also, to

calculate the gas-phase species concentrations by resolving diffusion equation Eq. (5). The parameters K_r and R_k are calculated according to the data of the temperature T and the concentrations C_k of the point of coordinates (x, z).

For a fixed value i and a variable value j, the development of Eqs. (2), (4) and (5) is of the form:

$$\alpha^i_{i,j-1}X^i_{j-1} + \alpha^i_{i,j}X^i_j + \alpha^i_{i,j+1}X^i_{j+1} = \beta^i_j \tag{10}$$

where parameters $\boldsymbol{\alpha^i_{j,j-1}}$, $\boldsymbol{\alpha^i_{j,j}}$, $\boldsymbol{\alpha^i_{j,j+1}}$, and $\boldsymbol{\beta^i_j}$are constants and parameters related to physical properties and numerical values of the discretized system.

It is clear to see the matrix form [A] × [X] = [B] of Eq. (10). The matrix [A] has the elements $\boldsymbol{\alpha^i_{j,j-1}}$, $\boldsymbol{\alpha^i_{j,j}}$, $\boldsymbol{\alpha^i_{j,j+1}}$ (which are not zero), the matrix (or vector) [B] has the element $\boldsymbol{\beta^i_j}$, and the matrix (or vector) [X] presents the unknown variable ($\mathbf{T^i_j}$, $\mathbf{U^i_j}$, or $\mathbf{C^i_{k,j}}$). For a fixed value i, this system of coupled equations is easily solved with the Gauss-Seidel (GS) method [46–48], and with the solution convergence test for values i and j, we have iterative calculation. For an iteration p, convergence is reached for absolute value $((X^{p+1}\text{-}X^p)/X^{p+1})$ lower than a limit value that is too small. This general form to solve equations is the Gauss-Seidel iterative method (GSIM).

The boundary conditions for components U and W of velocity vector $(\overrightarrow{V})$, temperature T, and concentrations C_k are as follows:

- In flow $(x = 0)$: $U = U_0$, $W = 0$, $T = T_0$; $C_k = C_{k,z} = 0$;
- Out flow $(x = L) : \left(\frac{\partial U}{\partial x}\right)_{x=L} = 0, \boldsymbol{W} = 0, \left(\frac{\partial T}{\partial x}\right)_{x=L} = 0, \left(\frac{\partial C}{\partial x}\right)_{x=L} = 0$;
- At filament $\left(x = X_{fil}, z = \frac{Z_{\max}}{2}\right)$: $\boldsymbol{U} = 0$, $\boldsymbol{W} = 0$, $\boldsymbol{T} = \boldsymbol{T}_{\text{fil}}$; the filaments are considered punctual without dimensions;
- At substrates ($z = Z$ or $z = Z_{max}$): $\boldsymbol{U} = 0$, $\boldsymbol{W} = 0$, $\boldsymbol{T} = \boldsymbol{T}_{\text{sub}}$, $\left(\frac{\partial C}{\partial x}\right)_{x=L} = 0$.

These boundary conditions give the elements of matrix [A] and matrix [B] corresponding to values of i and j.

To avoid the problems of singularities, we choose continuous functions for the initialization of the values of the components of the velocities and the initialization of the values of the temperatures. We choose a parabolic variation for U_0 (as function of z) and a linear variation for T_{sub} (as function of x) near the entrance of the reactor. To have the initialization of concentrations, we calculate them for each temperature from 300 to 2100 K; we use GSIM to solve equations for concentrations $C_{k,0}(i,j)$:

$$R_k = \sum \left(\pm K_r(T)[A_m]^{\alpha}\left[B_{m'}\right]^{\beta} \ldots \ldots\right) = 0 \tag{11}$$

We developed a numerical program using FORTRAN language; the general numerical scheme for calculation of T, U, W, and C_k is summarized in three stages as follows:

Stage 1: Initialization

- Initialization of T, U, W with continues values and according to boundary conditions

Stage 2: Calculation of T, U, W without variation of C_k

By a loop on index i, we have to:

(a) Calculate T by GSIM
(b) Calculate U by GSIM and correction of flux
(c) Calculate W from continuity equation
(d) Return to step (a) until convergence for all values i and j

Stage 3: Calculation of T, U, W, and C_k

The calculated values on step 2 are initial values for this step. By a loop on index i, we have to:

(a) Initialize T, U, W, and C_k
(b) Calculate T by GSIM
(c) Calculate U by GSIM and correction of flux
(d) Calculate W from continuity equation
(e) Calculate K_{reac} and D_k as a function of z (or index j)
(f) Calculate C_k for different k particles by GSIM
(g) Return to step (b) until convergence for all values i and j
(h) Take final results and calculate different parameters

Results and discussion

In this section, we present temperatures, velocities, and concentrations of molecules and radicals for a reactor with three filaments ($n = 3$) and four filaments ($n = 4$). Data values are $P_0 = 10^3$ Pa (7.5 Torr), $U_0 = 10$ mm/s, $T_{\text{fil}} = 2100$ K, $T_0 = 300$ K, and $T_{\text{sub}} = 1173$ K. Most results are for dimensions of the reactor: $Z_{\max} = 20$ mm, $L = 240$ mm, $D_{\text{ff}} = 50$ mm for $n = 3$ and $\text{Z}_{\max} = 20$ mm, $L = 240$ mm, $D_{\text{ff}} = 33.3$ mm for $n = 4$. The composition of the gas mixture is 05% of CH_4 and 95% of H_2. These values of filament temperature (2100 K) and gas mixture rate (05%, 95%) are according to data used in [15, 16, 31].

Distributions of velocity and temperature

In this subsection, we present distributions of temperature T and distributions of velocity components U and W for the cited values. A few characteristic planes are defined. The plane of the filaments is the horizontal plane carrying the filaments for $\text{z} = Z_{\max}/2$; the plane of a filament is the vertical plane containing a filament ($x = 7$ cm, 11.99 cm, 16.98 cm or $n = 3$ filaments and $x = 8.66$ cm, 11.99 cm, 15.30 cm, 18.61 cm for $n = 4$ filaments). We also define the vertical planes between filaments (example $x = 9.5$ cm for $n = 3$ filaments).

For $n = 3$, the calculations show that the temperature distributions at the hot filaments are identical; similarly, the temperature distributions between the hot filaments are identical. For $n = 4$, we have very similar curves and the conclusions are also identical. Figure 2 shows the distribution of the gas temperature as a function of z between filaments and at each filament for three and four filaments. The temperature distributions are symmetrical. The temperature takes a maximum value at the center of the reactor ($T_{\text{fil}} = 2100$ K, $z = Z_{\max}/2$) when the gas comes near to the hot filaments along the z direction, and then decreases gradually when the gas goes far away from the filaments

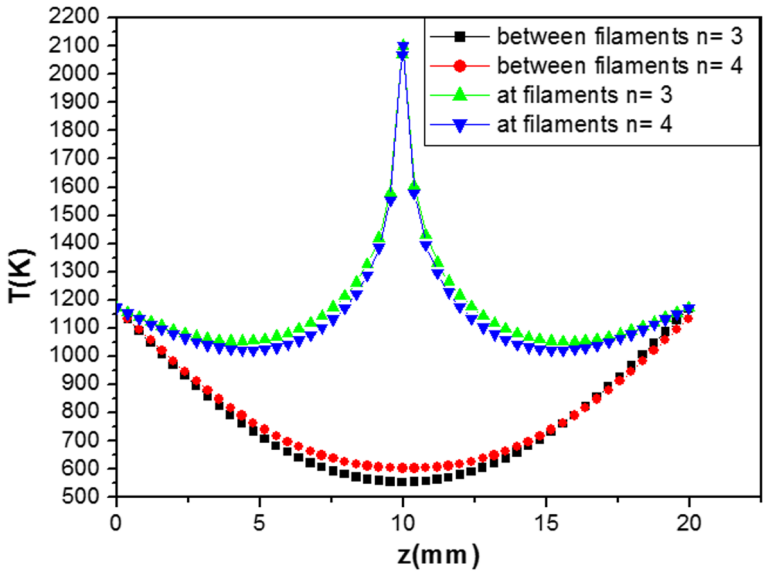

Fig. 2 Distribution of T as a function of z between filaments and at the filaments for $n = 3$ and for $n = 4$

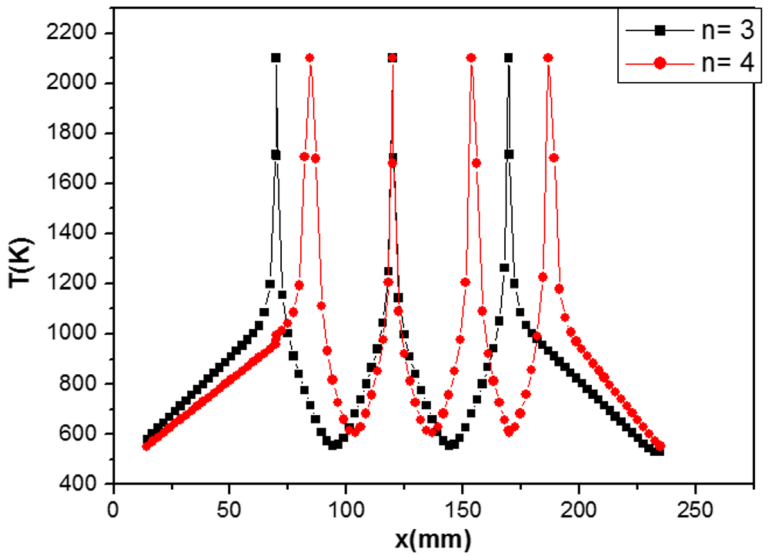

Fig. 3 Distribution of T as a function of x for $z = Z_{max}/2$ and for $n = 3$ and $n = 4$

(Fig. 2, at filaments). Between the filaments, temperature increases from 3 to 4 filaments by 11.46% (Fig. 2, between filaments). The temperatures in the central regions, around filaments, are more than the temperatures far from the filament region; this result confirms other results [49].

Figure 3 shows the distribution of the gas temperature as a function of x for horizontal filament plane ($z = Z_{max}/2$) for $n = 3$ and $n = 4$. The symmetry at the filaments and between the filaments is confirmed. The zones between filaments have a remarkable periodicity. The difference at the inlet of the reactor and the outlet is due to the initial conditions and the conditions of the fluid flow. Indeed, at the inlet of the reactor, the temperature of the gas is $T_0 = 300$ K and that of the substrate is $T_{sub} = 1173$

K; we have assumed a linear variation as a function of x at the first zone of the substrates. This choice of continuous function avoids the problems of singularities when solving the differential equations.

As for the temperature distributions, the calculations show that the distributions of components u and W of velocity as function of z at the filaments are identical. These distributions between the filaments are also identical. Figure 4 shows distribution of the component U of the velocity as a function of z between filaments and at the filaments for three filaments and four filaments. The increased gradient between the filaments was much larger than that in the filaments; the maximum value of velocity $U_{\max}$ is at 15.23 mm/s (for $n = 3$) and at 14.96 mm/s (for $n = 4$). Velocity distribution has near parabolic form far from filaments. For exact parabolic form $U_{\max} = (3/2)U_0$. The velocity reaches zero values on filaments by the severe interaction between filaments and the flow of viscous gas [31]. Between filaments, the value of $U_{\max}$ for 3 filaments is greater than that for 4 filaments by 2.98%. These results were consistent with what was found by Goodwin and Gavillet [16]: velocity distribution has a parabolic form far from filaments.

For three filaments and four filaments, the distribution of the component W of the velocity as a function of z is also symmetrical, between filaments and at the filaments.

Distributions of concentrations

In this subsection, we mainly present the concentrations of molecules and radicals in the reactor for $n = 3$ and $n = 4$.

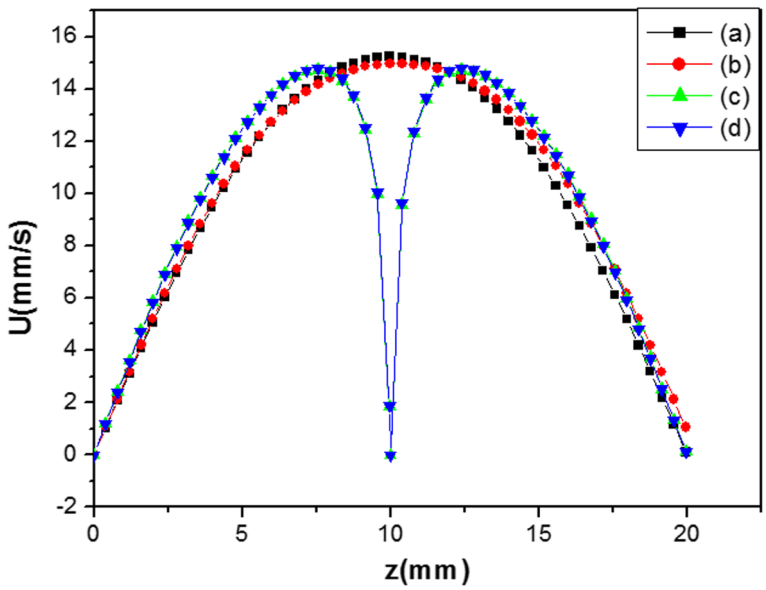

Fig. 4 Distribution of U as a function of z, between filaments for n=3 (**a**) and for n=4 (**b**) and at filaments for n=3 (**c**) and for n=4 (**d**)

Concentration of CH_3, H, and C_2H_5

Calculations show that the curve of concentration of each radical CH_3, H, or C_2H_5 is symmetrical and perfectly identical at the filaments. Between filaments, the curves of concentrations of these radicals are also symmetrical and identical.

Figure 5 shows the distributions of CH_3 radical concentration as function of z at the filaments and between the filaments for $n = 3$ and for $n = 4$. The curves are symmetrical. At the filaments, the comparison shows that the concentration for $n = 3$ is higher than that for $n = 4$; the difference varies from 1.59 to 1.79%. Between the filaments, the concentrations for $n = 4$ is higher than that for $n = 3$, and it is from 3.95 to 2.24%.

The calculation of concentrations of H, as a function of z at the filament for $n = 3$ and $n = 4$, shows that the concentrations have approximate values; the concentration for $n = 4$ is higher than that for $n = 3$, and the difference is from 1.31 to 0.86%. Between the filaments, the concentration for $n = 3$ is higher than that for $n = 4$; the difference is from 3.13 to 2.95%.

For C_2H_5 radical, the concentration for $n = 3$ is higher than that for $n = 4$; the difference is from 5.66 to 1.25% at the filaments. Between the filaments, the concentration for $n = 4$ is higher than that for $n = 3$; it varies from 61 to 17%.

Concentrations of CH_4, H_2, and other species C_2H_6, C_2H_4, C_2H_2, C_2H_3

Our calculations show that the distributions of concentration of C_2H_6, C_2H_4, C_2H_2, and C_2H_3, as a function of x, for filaments' plane ($z = Z_{max}/2$) and substrates ($z = 0$, $z = Z_{max}$) for $n = 4$ have the same remarks concerning forms and the symmetry as distributions of CH_3, H, and C_2H_5.

As it has shown before, the temperature curves are identical and superimposable at the level of the vertical planes containing the filaments (at filaments). At the median vertical planes between two successive filaments, the temperature curves or

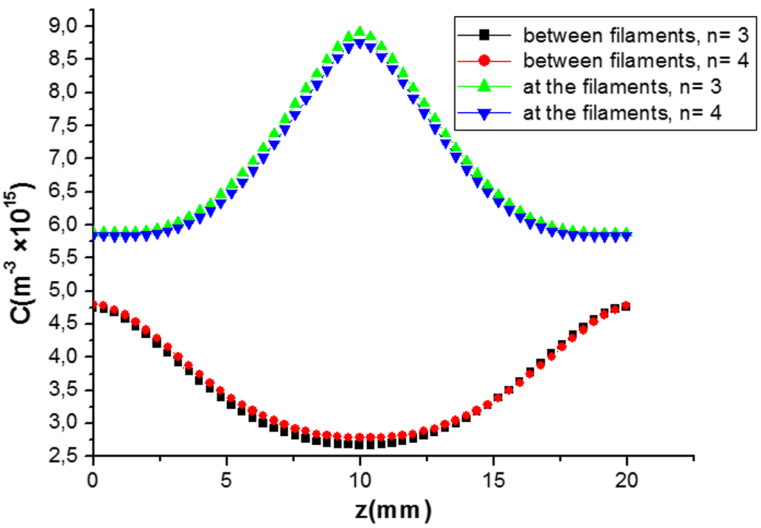

Fig. 5 Distribution of concentration of CH_3 as function of z; at the filaments and between the filaments

distributions are identical and superimposable. We have homogeneity or periodicity of the zones between two successive filaments. The distributions of velocity components U and W have the same shapes respectively component to component.

The distributions of the concentrations C_k of all the species ($k = 1,\ldots, 9$), as a function of z, have respectively identical curves at vertical planes containing the filaments (at filaments). We note the same remark for median vertical planes between filaments; there is homogeneity or periodicity of the zones between two successive filaments. This result is also linked to the choice of entry conditions for the gas mixture (U_0 and P_0) relative to the dimensions of the reactor (L, Z_{max}, D_{ff}). This choice gives a periodicity mainly for T, U, and W. These results have the same remarks for the concentrations which results are mainly dependent on the reaction constants $K_{\mathbf{reac}}$ and the diffusion coefficients D_k; the effect of temperature (filaments and substrates) is the most important. Debroy et al. [17] concluded that diffusion mechanisms are mostly responsible for both heat and mass transfer inside the HFCVD reaction chamber.

Figure 6 shows the concentrations C_k of the different molecules and radicals as a function of z, four $n = 4$, between the filaments (Fig. 6a–c) and at the filaments (Fig. 6b–d). There is an order in the presence of different species in the reactor; the molecules of H_2 and CH_4 are dominant. For CH_4 and between the filaments, the concentration for $n = 3$ is higher than that for $n = 4$; the difference is from 4.10 to 2.31%. At the filament, for $n = 3$ and $n = 4$, the concentrations have approximate values; the difference is about 1.21 to 0.73%.

The third species is ethane C_2H_6, in the order of 10^{18} m^{-3}. For the fourth and fifth order, there are C_2H_4 and C_2H_5 with close concentration values (10^{16} m^{-3} at 10^{15} m^{-3}). Contrary to the plasma enhanced chemical vapor deposition (PECVD) processes where the concentration of methyl CH_3 is high, here in HFCVD processes, the concentration of ethyl C_2H_5 is higher than that of CH_3. Other works [18–20] give concentration of CH_3 higher than those of C_2H_6, C_2H_4, and C_2H_5; this result is different from ours. We have shown in a conference presentation that in HFCVD processes, temperature is too high and the reaction rates which give heavy elements (C_2H_6, C_2H_4, C_2H_5) are more important. Indeed, chain reactions will allow consumption of CH_3 radicals by the reactions R6 and R7. We have in the sixth order CH_3 with a concentration less than 10^{15} m^{-3}. Although the hydrogen molecule H_2 is dominant, the atomic hydrogen H has a low concentration.

The initial concentrations of H_2 and CH_4 are respectively 2.29×10^{23} m^{-3} and 1.20×10^{22} m^{-3}, so 95% and 5% respectively. Inside the reactor, at the filaments' plane ($z = Z_{max}/2$), we note approximate rate of H_2 and CH_4 of 98.1% and 1.9% respectively; there is production of H_2 and consumption of CH_4. We note also approximate productions of C_2H_6 and C_2H_4, about 2.3×10^{-3}% and 3.6×10^{-5}% respectively. It is in the seventh order with a concentration of around 10^{15} m^{-3}. The concentration of C_2H_3 varies from 1.28×10^8 to 9.48×10^8 m^{-3}. In the last position, we have the radical C_2H_2 with a very low concentration (less than 10^{-2} m^{-3}).

Table 3 gives the average values of the concentrations of the different species near the substrates ($z = 0$ and $z = Z_{max}$) and at the plane of the filaments ($z = Z_{max}/2$); the average values are taken on the x range from 50 mm to 230 mm (to avoid the effects of the edges).

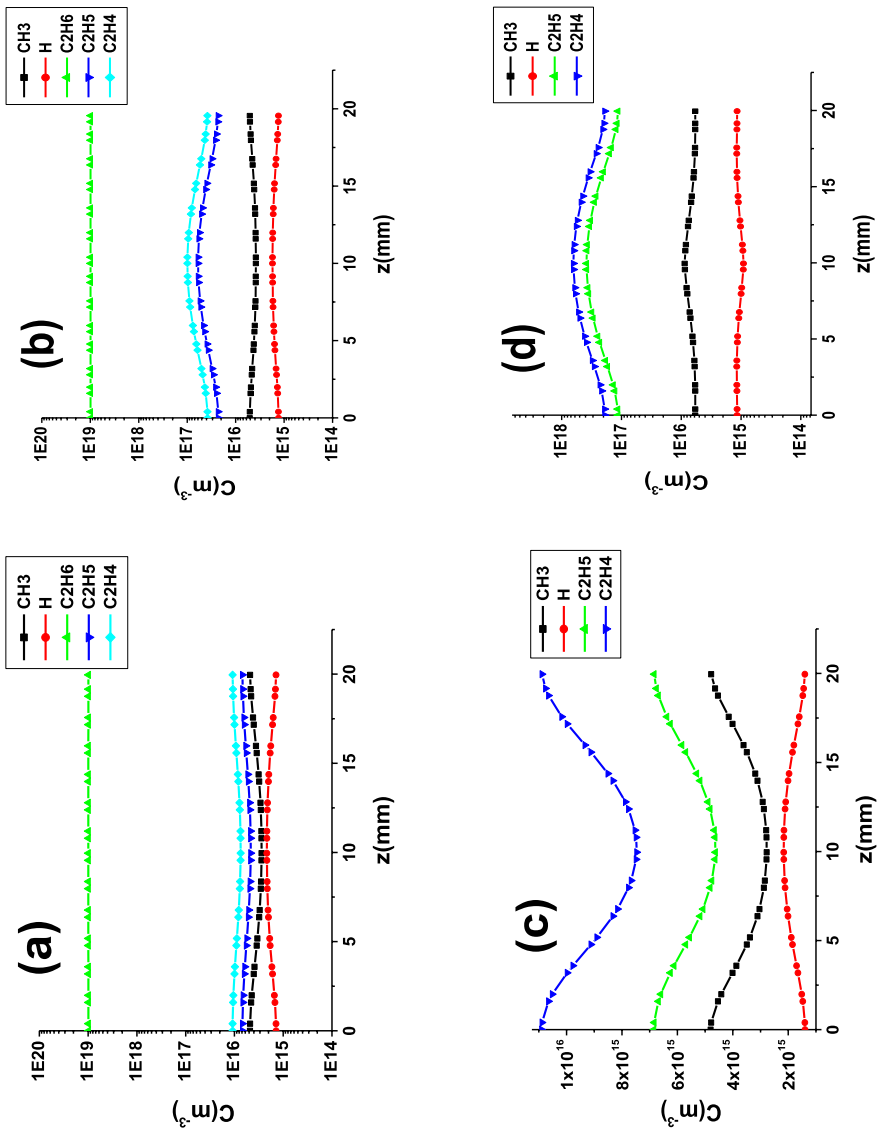

Fig. 6 Concentrations C_k of molecules and radicals as a function of z, for $n = 4$, **a**, **c** between the filaments, **b**, **d** at the filaments

Table 3 Average concentrations of species at the substrates and at the plane of the filaments

Molecule/radical	Average concentration $C_{k,av}$ (m^{-3}) for $n = 4$	
	Substrates $z = 0, z = Z_{max}$	Plane filaments $z = Z_{max}/2$
H_2	4.74×10^{23}	4.10×10^{23}
CH_4	6.70×10^{21}	7.94×10^{21}
C_2H_6	9.89×10^{18}	9.88×10^{18}
C_2H_4	5.25×10^{16}	1.50×10^{17}
C_2H_5	32.89×10^{15}	94.85×10^{15}
CH_3	5.16×10^{15}	4.29×10^{15}
H	1.28×10^{15}	1.64×10^{15}
C_2H_3	128.02×10^{6}	947.61×10^{6}
C_2H_2	0.0081	0.013

Table 4 Effect of the number of filaments on concentrations

	$D_{ff} = 50$ mm ($n = 3$)	$D_{ff} = 33.3$ mm ($n = 4$)
T_{min} (K)	554.3572	602.84
U_{max} (mm/s)	15.23	14.96
$C_{CH3,min}$ (m^{-3})	2.67×10^{15}	2.78×10^{15}
$C_{CH3,z=0}$ (m^{-3})	5.20×10^{15}	5.22×10^{15}
$C_{H,max}$ (m^{-3})	2.23×10^{15}	2.16×10^{15}
$C_{H,z=0}$ (m^{-3})	1.29×10^{15}	1.29×10^{15}
$C_{C2H5,min}$ (m^{-3})	1.79×10^{15}	4.63×10^{15}
$C_{C2H5,z=0}$ (m^{-3})	3.03×10^{16}	3.29×10^{16}

For real experiments, at the outlet of the reactor, the radicals C_2H_5, CH_3, and C_2H_3 and H should give stable molecules (H_2, CH_4, C_2H_6, C_2H_4, and C_2H_2). We think that this effect will not have too much influence on the results of our calculations nor the generality of the model used.

Effects of number of filaments and distance filaments-substrates

As we mentioned, the calculation shows the homogeneity and periodicity between the regions for $n = 3$ and for $n = 4$.

Table 4 shows the effect of number of filaments on concentrations of radicals H, CH_3, and C_2H_5. As the number of filaments increases, the distance between filaments decreases; heating energy input increases and the temperature of the gas increases. We observe that the production of CH_3 and C_2H_5 near the surface increases and at the same time the growth rate of the thin film will increase.

Table 5 presents the effect of distance filaments-substrates $Z_{max}/2$ on concentrations of radicals H, CH_3, and C_2H_5 for $n = 4$. The values of U_0 are taken to have similar flow velocities (U_{max} is of the order of 15 mm/s). The maximum values of the speeds and the minimum values of the temperatures are calculated at $Z_{max}/2$ and between filaments; the values of the concentrations are the average values taken for x varying from 50 to 230 mm. If the distance filaments-substrates increase, the average concentrations of CH_3

Table 5 Effect of distance filaments-substrates on concentrations for $n = 4$

	$Z_{max} = 12$ mm $U_0 = 6$ mm/s	$Z_{max} = 16$ mm $U_0 = 8$ mm/s	$Z_{max} = 20$ mm $U_0 = 10$ mm/s
$U_{max,zmax/2}$ (mm/s)	15.37	15.20	14.96
$T_{min,\ zmax/2}$ (K)	549.19	576.64	602.84
$C_{CH3,av,zmax/2}$ (m^{-3})	3.60×10^{15}	3.89×10^{15}	4.41×10^{15}
$\boldsymbol{C_{CH3,av,z=0}}$ (m^{-3})	4.41×10^{15}	4.81×10^{15}	5.20×10^{15}
$C_{H,av,zmax/2}$ (m^{-3})	1.83×10^{15}	1.74×10^{15}	1.61×10^{15}
$C_{H,z=0}$ (m^{-3})	1.46×10^{15}	1.36×10^{15}	1.28×10^{15}
$C_{C2H5,av,zmax/2}$ (m^{-3})	6.58×10^{16}	7.40×10^{16}	9.77×10^{16}
$C_{C2H5,av,z=0}$ (m^{-3})	2.50×10^{16}	2.70×10^{16}	3.40×10^{16}

and C_2H_5 increase and the average concentrations of H decreases. The effects of chemical reactions and temperature in volume are the most important.

Concentrations of CH_3, C_2H_5, and H near the substrates

In our calculations of the concentrations in volume, we did not consider the deposition and the interaction of particles with the surface. This assumption will not significantly influence concentrations in the volume, the amount deposited is too low compared to the initial amount: this is the effect of the bath in physics.

The temperature of the substrate is $T_{sub} = 1173$ K. Near the substrates, the average concentrations of H and CH_3 are practically constant for $n = 3$ and $n = 4$; the concentration ratio $C_H/(C_H + C_{CH3})$ is 20%. The concentration of C_2H_5 is 4.5 greater than that of H and CH_3 for $n = 3$, and it is 5.1 greater than that of H and CH_3 for $n = 4$.

The type of substrates plays an important role in the growth of thin film. A growth rate can be estimated by proposing a diamond layer growth with a given sticking coefficient. We consider sticking coefficients $S_H = 0.01$, $S_{CH3} = 0.11$, and $S_{C2H5} = 0.07$ of H, CH_3, and C_2H_5 respectively [16, 32, 50]. For particles k of mass m_k at temperature near substrate $T_{nS} = T_{sub}$, we calculate the most probable thermal velocity [51]:

$$V_k - = \sqrt{\frac{2K_b T_{ns}}{m_k}} \tag{12}$$

For diamond carbon thin film, we can estimate the value of growth rate G_k resulting from the radical k. An approximate formula of G_k is:

$$G_k = \frac{1}{d} C_{k,av} \times \left(\frac{1}{6} V_k\right) \times S_k \times m_{kd} \tag{13}$$

where, for radicals H, CH_3, and C_2H_5, $C_{k,av}$ is the average concentrations, S_k is the sticking coefficient, and $m_{kd}$is the mass of the deposited radical (m_{kd} is not necessarily m_k, because of the hydrogen atoms which release sites from the surface). d is volumetric mass density of diamond carbon.

Table 6 presents values of growth rate G, from some values of U_0 and some values of distance filaments-substrates $Z_{max}/2$.

For average value $d = 3.51$ g/cm^3 and with two radicals H and CH_3, for the same values $Z_{max} = 20$ mm $U_0 = 10$ mm/s, calculated maximum values of growth rate G_{max} are

Table 6 Values of growth rate *G* for some values of Z_{max}

Growth (μm/h)	$n = 3$ $Z_{max} = 20$ mm $U_0 = 10$ mm/s	$n = 4$ $Z_{max} = 20$ mm $U_0 = 10$ mm/s	$n = 4$ $Z_{max} = 16$ mm $U_0 = 8$ mm/s	$n = 4$ $Z_{max} = 12$ mm $U_0 = 6$ mm/s
G_{CH3}	2.20×10^{-3}	2.21×10^{-3}	2.06×10^{-3}	1.88×10^{-3}
G_{C2H5}	1.13×10^{-2}	1.29×10^{-2}	1.05×10^{-2}	9.80×10^{-3}
$G=G_{CH3}+G_{C2H5}$	1.35×10^{-2}	1.51×10^{-2}	1.22×10^{-2}	1.15×10^{-2}

0.0022 μm/h for $n = 3$ and 0.00221 μm/h for $n = 4$. For a given number of filaments (example $n = 4$), when Z_{max} decreases, there is not necessarily an increase in the growth rate. These results are smaller than other theoretical and experimental works. The values of growth rate are about 0.4 μm/h in work [18] and less than 0.2 μm/h in [20]. Taking into account the presence of C_2H_5, for same values $Z_{max} = 20$ mm $U_0 = 10$ mm/s, calculated deposition rates (0.0135 μm/h for $n = 3$ and 0.0151 μm/h for $n = 4$) are lower than the values recorded in the experiments.

We can use the Hertz- Knudsen equation [52, 53] to estimate the flux of particles which collide with surface. For a particle of mass *m*, at temperature *T*, and in pressure *P*, the flux ϕ is [52]:

$$\varphi = \frac{P}{\sqrt{2\pi \times m \times K_b \times T}} \tag{14}$$

From values of flux, growth rate can be estimated for a sticking coefficient S_k and for diamond carbon density *d*.

The comparison of growth rate is not so reliable because of the differences in volume concentrations (gas temperature) and velocities of radicals near surfaces (substrate temperature). The expression of growth rate *G* used here and in other expressions do not respond to the complexity of the phenomena of deposition. Knowledge of the sticking coefficients of radicals is not sufficient, nor even the coefficients of all radicals and molecules. It would be important to know the rate of coverage of the surface with hydrogen atoms. Otherwise, it is necessary to know the free sites occupied by the hydrogen atoms. A calculation taking into account the recombination coefficients and sticking coefficients of all the radicals and molecules, as well as the occupancy rate in H, would give a more reliable result and would be close to the experimental results. Experimental measurements of the production of stable molecules (C_2H_6, C_2H_4, and C_2H_2) would make it possible to better understand the mechanisms and correct the different models.

Conclusions

In this work, we have presented a two-dimensional model for HFCVD for CH_4/H_2 gas mixture in a reactor with three and four filaments. This model describes the phenomena that occur in the reaction chamber of a reactor and the effect of the number of filaments and their position in relation to the substrate. The proposed reactor gives identical distributions of temperatures, velocities, and concentrations at the filaments and also between the filaments; the different regions between filaments show great homogeneity and remarkable periodicity. The results show that if the temperature of gas increases, the production of CH_3 and C_2H_5 near the surface increases and the growth rate of the

thin film increases. The calculations show that concentrations of C_2H_6, C_2H_4, and C_2H_5 are very high. The diffusion phenomena related to temperatures and the rates of chemical reactions also related to temperatures constitute the most important aspects of the dynamics of concentrations in gas.

The study of the growth of the thin film is very complex. In fact, it requires more detailed studies on the coefficients of sticking and recombination of the species and on the rate of occupation of the sites by the hydrogen atom at the deposit surface. Experimental measurements of the production of stable molecules (C_2H_6, C_2H_4 and C_2H_2) would make it possible to better understand the mechanisms.

Nomenclature

$[A_i]$, $[B_i]$ Species concentrations, m^{-3}
a_i, b_i Stoichiometric coefficients of chemical reactions
A_r Constant, mol cm^{-3} s^{-1}
C_k Concentration of each radical or molecule, m^{-3}
$C_{k,av}$ Average concentrations, m^{-3}
C_p Specific heat, J kg^{-1} K^{-1}
C_{tot} Total concentration, m^{-3}
d Volumetric mass density, g/cm^3
D_{ff} Distance between filaments, mm
D_k Diffusivity of species, m^{-3}
D_{mk} Diffusion coefficients of the neutral species k, m^2/s
E_a Activation energy, K_J mol^{-1}
G_k Growth rate, μm/h
g_x Gravity force component in the x direction, m s^{-2}
g_z Gravity force component in the z direction, m s^{-2}
k Number radical or molecule
K_b Boltzmann constant, J K^{-1}
K_r Chemical rate constants, m^3/s
L Length of the reactor in the x direction, mm
m_{kd} Mass of the deposited radical, g
M_{mk} Reduced mass, kg
n Number of filaments
N_a Avogadro constant, mol^{-1}
P Gas pressure, Pa
P_0 Initial pressure, Pa
R Universal gas constant, J mol^{-1} K^{-1}
R_k Rate production, m^{-3} s^{-1}
S_k Sticking coefficients
T_0 Initial temperature, K
T Temperature of gas, K
T_{fil} Filament temperature, K
T_{nS} Temperature near substrate, K
T_{sub} Substrate temperature, K
U_0 Initial velocity, mm/s

U Velocity component in the x direction, mm/s
$\overrightarrow{V}$ Gas velocity vector, mm/s
V_k Most probable thermal velocity of particle k
W Velocity component in the z direction, mm/s
x Cartesian axis directions, mm
X_{fil} Filament position
z Cartesian axis directions, mm
Z_{max} Distance between substrates, mm
Greek symbols
β Constant
μ Dynamic viscosity, N s m^{-2}
ρ_0 Volume density, m^{-3}
λ Heat transfer efficiency, W m^{-1} K^{-1}
σ_{mk} Binary collision diameter, Å
$\varepsilon_m, \varepsilon_k$ Lennard-Jones parameters K
ϕ Flux of the gas molecules, m^{-2} s^{-1}
Special symbols
i Unitary vector in the x direction
j Unitary vector in the z direction
$\overrightarrow{grad}$ Differential operator
div Differential operator
$\frac{\partial}{\partial x}, \frac{\partial}{\partial z}$ Partial derivatives
∇ Nabla mathematical operator
[A],[X],[B] Matrix for Gauss-Seidel calculation
$\alpha^i_{j,j-1}, \alpha^i_{j,j}, \alpha^i_{j,j+1}, \beta^i_j$ Elements of matrix [A] and the matrix [B]
$\Omega_D(T^*)$, A_D, B_D,C_D, D_D, E_D, F_D, G_D, H_D Dimensionless collision integral function of the temperature and its parameters

Abbreviations

a-C:H	Amorphous hydrogenated carbon
HFCVD	Hot filament chemical vapor deposition
CH_4	Methane gas
H_2	Hydrogen gas
LED	Light-emitting diode
CVD	Chemical vapor deposition
PECVD	Plasma enhanced chemical vapor deposition
FVM	Finite volume method
av	Average

Acknowledgements
Our acknowledgments go to the responsible in charge of the Computer Resources Center (CRI) of Kasdi Merbah Ouargla University (UKMO) where part of the calculations were made. The authors acknowledge also the Directorate General of Scientific Research and Technological Development (DGRSDT) and the Thematic Science and Technology Research Agency (ATRST) who have given their support to the Laboratory LRPPS.

Authors' contributions
FK proposed the subject of this work which is the principal axis NK's doctoral thesis under the supervision of FK. The modelization, the interpretation, and the redaction of the manuscript were done by NK, FK, and OB. The numerical methods and the calculations are realized by NK. All authors read and approved the final manuscript.

Funding
No funding was obtained for this study.

Availability of data and materials
All data generated or analyzed during this study are included in this published article and are available from the corresponding author.

Declarations

Competing interests
The authors declare that they have no competing interests.

Received: 11 April 2022 Accepted: 12 July 2022
Published online: 19 August 2022

References

1. Sattam A, Krishna NM, Shashi P (2018) Stability of hydrogenated amorphous carbon thin films for application in electronic devices. Diam Relat Mater 90:172–180. https://doi.org/10.1016/j.diamond.2018.10.016
2. Mohamad F, Hanib NM, Uzer Noor UM, Rusop M (2010) Properties of amorphous carbon thin films for solar cell applications. AIP Conf Proc 1217:140–146. https://doi.org/10.1063/1.3377800
3. Grenadyorov AS, Oskomov KV, Solovyev AA (2018) Effect of deposition conditions on optical properties of a-C:H:SiOx films prepared by plasma-assisted chemical vapor deposition method. Optik 172:107–116. https://doi.org/10.1016/j.ijleo.2018.07.024
4. Soga T, Jimbo T, Krishna KM, Umeno M (2000) Amorphous carbon thin films for optoelectric device application. Int J Modern Phys B 14:206–217. https://doi.org/10.1142/S0217979200000200
5. Alix G, Khaled H, François S, Jocelyn A (2001) CVD diamond films: from growth to applications. Curr Appl Phys 1:479–496. https://doi.org/10.1016/S1567-1739(01)00061-X
6. Enric B, Markus AMH (eds) (2011) Synthetic diamond films. Book News-Inc, Canada
7. Lothar S, Markus H, Roland K (2006) The versatility of hot-filament activated chemical vapor deposition. Thin Solid Films 515:1017–1024. https://doi.org/10.1016/j.tsf.2006.07.073
8. Khmelnitskiy RA (2015) Prospects for the synthesis of large single-crystal diamonds. Physics-Uspekhi 58:134–159
9. Liu H, Dandy DS (1995) Studies on nucleation process in diamond CVD: an overview of recent developments. Diam Relat Mater 4:1173–1188. https://doi.org/10.1016/0925-9635(96)00297-2
10. Tamilla MA (2002) Mathematical modeling of plasmachemical processes. Turk J Phys 26:415–426 https://journals.tubitak.gov.tr/physics/abstract.htm?id=5852
11. Waqar A, Sein H, Malcolm J, Rego C, Israr Ul H, Karthikeyan S, Javad Y (2012) Emerging nanotechnologies in dentistry, processes, materials and applications. Elsevier Inc, Norwich
12. Jansen F, Machonkin MA, Kuhman DE (1990) The deposition of diamond films by filament techniques. J Vac Sci Technol 8:3785–3790. https://doi.org/10.1116/1.576494
13. Amaral M (2013) Diamond based materials for biomedical applications. Woodhead, USA
14. Shenderova OA, Gruen DM (2012) Ultrananocrystalline diamond: synthesis, properties and applications. Elsevier Inc, Britain
15. Olivas-Martinez M, Pérez-Tello M, Cabanillas-Lopez R, Contreras-Lopez O, Soto-Herrera G, Castillon-Barraza F (2007) A computational model for the hot-filament chemical vapour deposition process to produce diamond films. Simul Mater Sci Eng 15:237–261. https://doi.org/10.1088/0965-0393/15/3/004
16. Goodwin DG, Gavillet GG (1990) Numerical modeling of the filament-assisted diamond growth environment. J Appl Phys 68:6393–6400. https://doi.org/10.1063/1.346858
17. Debroy T, Tankala K, Yarbrough WA, Messier R (1990) Role of heat transfer and fluid flow in the chemical vapor deposition of diamond. J Appl Phys 68:2424–2432. https://doi.org/10.1063/1.346502
18. Kondoh E, Ohta T, Mitomo T, Ohtsuka K (1992) Experimental and calculational study on diamond growth by an advanced hot filament chemical vapor deposition method. J Appl Phys 72:705–711. https://doi.org/10.1063/1.351856
19. Kondoh E, Ohta T, Mitomo T, Ohtsuka K (1999) Surface reaction kinetics of gas-phase diamond growth. J Appl Phys 73:3041–3046. https://doi.org/10.1063/1.353011
20. May PW, Harvey JN, Smith JA, Mankelevich YUA (2006) Reevaluation of the mechanism for ultrananocrystalline. Diamond deposition from $Ar/CH_4/H_2$ gas mixtures. J Appl Phys 99:104907. https://doi.org/10.1063/1.2195347
21. Frenklach M, Wang H (1991) Detailed surface and gas-phase chemical kinetics of diamond deposition. Phys Rev B 43:1520–1545. https://doi.org/10.1103/PhysRevB.43.152
22. McMaster MC, Hsu WL, Coltrin ME, Dandy DS (1994) Experimental measurements and numerical simulations of the gas composition in a hot-filament-assisted diamond chemical-vapor-deposition reactor. J Appl Phys 76:7567–7577. https://doi.org/10.1063/1.358525
23. Mankelevich YA, Rakhimov AT, Suetin NV (1996) Two-dimensional simulation of a hot-filament chemical vapor deposition reactor. Diam Relat Mater 5:888–894. https://doi.org/10.1016/0925-9635(95)00493-9
24. Mankelevich YA, Rakhimov AT, Suetin NV (1998) Three-dimensional simulation of a HFCVD reactor. Diam Relat Mater **7**:1133–1137. https://doi.org/10.1016/S0925-9635(98)00163-0
25. Wolden C, Gleason KK (1993) Heterogeneous formation of atomic hydrogen in hot-filament diamond deposition. J Appl Phys Lett 62:2329–2331. https://doi.org/10.1063/1.109407
26. Zuo W, Shen B, Sun FH, Chen M (2008) Simulation of substrate temperature distribution in diamond films growth on cemented carbide inserts by hot filament CVD. Appl Mech Mater 10-12:864–868. https://doi.org/10.4028/www.scientific.net/AMM.10-12.864

27. Cheng L, Zhang J, Wang X, Zhang T, Shen B, Sun F (2014) Simulation of temperature distribution in HFCVD diamond films growth on WC-Co drill tools in large quantities. Key Eng Mater 589-590:399–590. https://doi.org/10.4028/www.scientific.net/KEM.589-590.399
28. Tankala K, DebRoy T (1993) Transport phenomena in the scale-up of hot filament-assisted chemical vapor deposition of diamond. Surf Coat Technol 62:349–355. https://doi.org/10.1016/0257-8972(93)90266-Q
29. Song GH, Sun C, Huang RF, Wen LS (2000) Simulation of the influence of the filament arrangement on the gas phase during hot filament chemical vapor deposition of diamond films. J Vac Sci Technol A 18:860–863. https://doi.org/10.1116/1.582267
30. Song GH, Sun C, Huang RF, Wen LS (1999) The simulation of the space fields of gas physical parameters during HFCVD diamond films. Acta Metall Sin 35(6):648–653
31. Wang AY, Lee KR, Sun C, Wen LS (2006) Simulations of the dependence of gas physical parameters on deposition variables during HFCVD diamond films. J Mater Sci Technol 22(5):559–604
32. Menningen KL, Childs MA, Anderson LW, Lawler JE (1996) Gas temperature in a hot filament diamond chemical vapor deposition system. Rev Sci Instrum 67:1546–1554. https://doi.org/10.1063/1.1146886
33. Park S (1999) Numerical modeling of diamond growth environment in HFCVD reactors. Met Mater 5:225–229. https://doi.org/10.1007/BF03026071
34. Eckert M, Neyts E, Bogaerts A (2008) Molecular dynamics simulations of the sticking and etch behavior of various growth species of (ultra) nanocrystalline diamond films. Chem Vap Depos 14:213–223. https://doi.org/10.1002/cvde.200706657
35. Tao Z, Yizheng Q, Shu W, Guodong H, Lijun Z, Zhe X (2019) Influence of the heat dissipation mode of long-flute cutting tools on temperature distribution during HFCVD diamond films. Crystals 9:394. https://doi.org/10.3390/cryst9080394
36. Rebrov A, Plotnikov M, Mankelevich Y, Yudin I (2018) Analysis of flows by deposition of diamond-like structures. Phys Fluids 30:016106. https://doi.org/10.1063/1.4996067
37. Gorbachev YE, Leshchev DV, Plotnikov MY, Rebrov AK, Yudin B (2019) Comparison of continual and molecular modeling of gas flow for diamond deposition. Conf Ser 1382:012152. https://doi.org/10.1088/1742-6596/1382/1/012152
38. Joseph L (1998) Le génie chimique à l'usage des chimistes. Librairie Tho, Paris
39. Schäfer L, Höfer M, Kröger R (2006) The versatility of hot-filament activated chemical vapor deposition. Thin Solid Films 515:1017–1024. https://doi.org/10.1016/j.tsf.2006.07.073
40. Koutlas GN, Vlachos NS (2003) Numerical modeling of pyrolytic laser-induced chemical vapor deposition. J Appl Phys 93:3049–3056. https://doi.org/10.1063/1.1543230
41. Strunin VI, Lyakhov AA, Khudaĭbergenov GZH, Shkurkin VV (2002) Numerical simulation of silane decomposition in an RF plasma. Tech Phys 47:760–766. https://doi.org/10.1134/1.1486201
42. Perrin J, Leroy O, Bordage MC (1996) Cross-sections, rate constants and transport coefficients in silane plasma chemistry. Contrib Plasma Phys 36:3–49. https://doi.org/10.1002/ctpp.2150360102
43. Babahani O, Khelfaoui F (2012) Calcul des concentrations de molécules et de radicaux lors de déposition de couches minces a-Si:H par procédés PECVD. Ann Sci Technol 4(2):115–120 https://journals.univ-ouargla.dz/index.php/AST/article/view/291
44. Herrebout D, Bogaerts A, Yan M, Gijbels R, Goedheer W, Dekempeneer E (2001) One-dimensional fluid model for an rf methane plasma of interest in deposition of diamond-like carbon layers. J Appl Phys 90:570–579. https://doi.org/10.1063/1.1378059
45. Versteeg HK, Malalasekera W (eds) (1995) An introduction to computational fluid dynamics the finite volume method. Longman Group Ltd, Harlow-England
46. Sibony M, Mardon JC (eds) (1984) Analyse numérique II, Approximations et équations différentielles. Editeurs des Sciences et des Arts, Paris
47. Barrand JP, Sacadura JF (eds) (1993) Initiation aux transferts thermiques. CAST, Lyon
48. Pu B, Yuan (2009) The alternate iterative Gauss-Seidel method for linear systems. Conf Ser 1411:012008. https://doi.org/10.1088/1742-6596/1411/1/012008
49. Wang AY, Sun C, Cao HA, Ji AL, Huang RF, Wen LS (2004) Two-dimensional simulations of temperature fields of the reactor wall during hot-filament CVD diamond film growth over a large area. Model Simul Mater Sci Eng 12:325–335. https://doi.org/10.1088/0965-0393/12/2/012
50. Von Keudell A, Meier M, Hopf C (2002) Growth mechanism of amorphous hydrogenated carbon. Diam Relat Mater 11:969–975. https://doi.org/10.1016/S0925-9635(01)00553-2
51. Moisan M, Pelletier J (eds) (2006) Physique des plasmas collisionnels application aux décharges haute fréquence. EDP Sciences, France
52. Kolasinski KW (ed) (2012) Surface science: foundations of catalysis and nanoscience. Wiley, USA
53. Persad AH, Ward CA (2016) Expressions for the evaporation and condensation coefficients in the Hertz-Knudsen relation. Chem Rev 116:7727–7776. https://doi.org/10.1021/acs.chemrev.5b00511

Publisher's Note